

Quantum phase transition in an effective three-mode model of interacting bosons

H. M. Frazão,^{1,2,*} J. G. Peixoto de Faria,³ G. Q. Pellegrino,³ and M. C. Nemes²

¹*Universidade Federal do Piauí, Campus Profa. Cinobelina Elvas, Bom Jesus, PI, Brazil*

²*Departamento de Física, Instituto de Ciências Exatas,
Universidade Federal de Minas Gerais, Belo Horizonte, MG, Brazil*

³*Departamento de Matemática, Centro Federal de Educação
Tecnológica de Minas Gerais, Belo Horizonte, MG, Brazil.*

(Dated: October 15, 2018)

Abstract

In this work we study an effective three-mode model describing interacting bosons. These bosons can be considered as exciton-polaritons in a semiconductor microcavity at the magic angle. This model exhibits quantum phase transition (QPT) when the parameters of the corresponding Hamiltonian are continuously varied. The properties of the Hamiltonian spectrum (*e.g.*, the distance between two adjacent energy levels) and the phase space structure of the thermodynamic limit of the model are used to indicate QPT. The relation between spectral properties of the Hamiltonian and the corresponding classical frame of the thermodynamic limit of the model is established as indicative of QPT. The average number of bosons in a specific mode and the entanglement properties of the ground state as functions of the parameters are used to characterize the order of the transition and also to construct a phase diagram. Finally, we verify our results for experimental data obtained for a setting of exciton-polaritons in a semiconductor microcavity.

* heliques@ufpi.edu.br

I. INTRODUCTION

One issue of great interest in condensed matter physics today is quantum phase transition (QPT) [1]. Differently from the usual thermodynamic phase transition, which is guided by thermodynamic fluctuations and characterized by a critical temperature, a QPT can be observed for $T = 0$ and is conducted by quantum fluctuations. The change in the system due to a QPT is observed when some parameter of the Hamiltonian is varied, rather than temperature as in the thermodynamic phase transition. As a simple example, we have the quantum Ising model in a transverse field, where a QPT is observed between ferromagnetic and paramagnetic phases when the intensity of the applied field is varied [1, 2]. As this example illustrates, the study of QPT conveys a better understanding of the complex behavior shown by many-body systems. This study can cross very different systems as, for example, systems involving light-matter interactions, such as cavity arrays coupled by optical fibers [3], or a two-species condensate of interacting bosons trapped in optical lattices [4]. The next paragraphs present other instances where QPT in many-body problems is considered and which are of interest for this work.

One of the systems under intense attention in recent decades is the semiconductor microcavity [5]. In this system, the interaction between cavity photons and excitons belonging to the semiconductor gives rise to a new *quasi*-particle called exciton-polariton [6]. There are many interesting features shown by this system as, for example, the superfluidity [7], and the generation of a Bose-Einstein condensate (BEC) in a solid state system [8] (which occurs even at room temperature [9]). Another interesting feature is the so-called *magic angle* configuration in which we observe a parametric amplification of the emitted light [10]. One possible theoretical description of this feature is given by considering only three modes for the exciton-polaritons, denominated *pump*, *signal* and *idler* [11]. The evidences pointed by experiment [10] suggest that only these three modes are coherently and macroscopically populated [5, 11]. In this situation one can approximate the Hamiltonian of the system by an effective three-mode Hamiltonian as we do in this work.

The experimental observation of QPT in the scope of condensed matter physics has been boosted by the development of techniques that allowed for the storage and handling of matter at the atomic level. In the past two decades, intense research has been done on systems of interacting trapped bosons, especially cold atoms trapped in optical lattices [12].

The interest in such systems is assigned to their capacity to simulate many phenomena predicted to occur in arrangements of trapped atoms, such as the BEC itself [13], solitons [14], bosonic Josephson effect, and nonlinear oscillations [15], and also a QPT from a Mott-insulator-like phase to a superfluid-like one [1, 16]. For a two-well condensate [17] or a three-well condensate [18, 19], the transition is between two dynamical regimes: macroscopic self-trapping and Rabi (or Josephson) oscillations [20]. These kinds of systems are generally described by a Bose-Hubbard-type Hamiltonian [21–23]. In this work we study an effective three-mode Hamiltonian essentially different from a Bose-Hubbard Hamiltonian but which exhibits a QPT between two phases: the macroscopic self-trapping (MST), characterized by the vanishing of the tunneling between the modes, and a regime of oscillations (RO), where tunneling is present.

In recent years, also classical analyses involving the thermodynamic limit of some quantum many-body models have contributed to the investigations of QPT. These analyses come to add themselves to other valuable tools to investigate QPT, many of them referring to the properties of the spectrum of the corresponding quantum Hamiltonian, as the level approximation (crossing), or to the measurement of entanglement of the ground state [24] near the critical point. Different systems were studied in this quantum-classical context, *e.g.*, the Lipkin model [25] and the pairing model [26] (both in nuclear physics), the Dicke model for superradiance in quantum optics [27], excitons in semiconductor bilayer electron systems [28], ultracold Bose gases trapped in multiple wells [19], among others [29]. In parallel with the quantum treatment, we perform as well the classical limit analysis to study QPT in the effective three-mode model for a system of interacting bosons. Our analysis results in a close analogy between some aspects of the spectrum of the quantum Hamiltonian and classical properties of the corresponding thermodynamic limit of the model. As an example, the different phases in the quantum regime are related to the existence of closed orbits in the classical thermodynamic limit. In fact, the MST phase corresponds to the situation in which there are no closed orbits in phase space, whereas the RO phase is characterized by the presence of such orbits. In this way, separatrices delimiting regions of the phase space characterized by different dynamical regimes in the classical limit are identified with the presence of non-trivial minima in the separation of adjacent energy levels. Besides that, the properties of the ground state are used to characterize the order of the transition and also to construct a phase diagram that shares some similarity with the phase diagram obtained for

the Lipkin model [25]. Our results can be applied to describe a system of exciton-polaritons in a semiconductor microcavity at the magic angle.

This work is organized as follows. In Sec. II, the effective Hamiltonian is presented and, in Sec. III, its spectral properties are shown; in Sec. IV, the classical thermodynamic limit of the Hamiltonian is taken and the resulting phase space is analyzed. In Sec. V, we discuss the QPT and a phase diagram. In Sec. VI, we verify our results for exciton-polaritons in a semiconductor microcavity, based on available experimental data. Finally, we present our conclusions in Sec. VII.

II. THREE-MODE APPROXIMATION FOR INTERACTING BOSONS

The starting point of this work is a three-mode Hamiltonian for interacting bosons in the form

$$H = \sum_{i=0,1,2} E_i a_i^\dagger a_i + \sum_{i+j=k+l} \hbar G_{ijkl} a_i^\dagger a_j^\dagger a_k a_l, \quad (1)$$

where a_i^\dagger (a_i) is the creation (annihilation) operator for a boson with energy E_i . The first term describes the free bosons while the second one describes the interaction between different bosonic modes which obeys the condition: $G_{ijkl} \neq 0$ for $i + j = k + l$, $G_{ijkl} = 0$ for $i + j \neq k + l$. As we see in the following, we can obtain a Hamiltonian as Eq. (1) for the description of exciton-polaritons in a semiconductor microcavity at the magic angle (Sec. II.A). An effective Hamiltonian (Sec. II.B) can be obtained from Eq. (1) by using the conservation of total number of bosons and the condition $i + j = k + l$ which means conservation of momentum for exciton-polaritons.

A. Exciton-polaritons in a semiconductor microcavity at the magic angle

An exciton-polariton is a *quasi*-particle formed from the coupling between an exciton and a photon in a semiconductor microcavity. Under certain experimental conditions we can model the exciton-polaritons in a semiconductor microcavity by the Hamiltonian [5, 11]

$$H = \sum_{\mathbf{k}} \hbar \Omega_{\mathbf{k}} p_{\mathbf{k}}^\dagger p_{\mathbf{k}} + \frac{1}{2} \sum_{\mathbf{k}, \mathbf{k}', \mathbf{q}} V_{\mathbf{k}, \mathbf{k}', \mathbf{q}}^{PP} p_{\mathbf{k}+\mathbf{q}}^\dagger p_{\mathbf{k}'-\mathbf{q}}^\dagger p_{\mathbf{k}} p_{\mathbf{k}'}, \quad (2)$$

where $p_{\mathbf{k}}^\dagger$ ($p_{\mathbf{k}}$) is the creation (annihilation) operator for an exciton-polariton with in-plane wave-vector \mathbf{k} and energy $\hbar \Omega_{\mathbf{k}}$. The first term describes the free exciton-polaritons while the

second one describes the interaction between different exciton-polariton modes. For typical values of the experimental parameters, the interaction coefficients are given by

$$V_{\mathbf{k},\mathbf{k}',\mathbf{q}}^{PP} \simeq V_0 u_{|\mathbf{k}'-\mathbf{q}|} u_{\mathbf{k}} \cdot u_{|\mathbf{k}+\mathbf{q}|} u_{\mathbf{k}'}, \quad V_0 = \frac{6e^2 a_{\text{exc}}}{\epsilon_0 A}, \quad (3)$$

where a_{exc} is the two-dimensional Bohr radius of the exciton-polariton, ϵ_0 is the dielectric constant of the semiconductor and A is the macroscopic quantization area. The $u_{\mathbf{k}}$'s are the so-called Hopfield coefficients, given by

$$u_{\mathbf{k}} = \left(\frac{\Delta_{\mathbf{k}} + \sqrt{\Delta_{\mathbf{k}}^2 + \Omega_R^2}}{2\sqrt{\Delta_{\mathbf{k}}^2 + \Omega_R^2}} \right)^{1/2}, \quad (4)$$

where $\Delta_{\mathbf{k}} = E_{\text{cav}}(k) - E_{\text{exc}}(k)$ is the detuning between the energies of cavity photons and excitons.

At the magic angle configuration, the system exhibits a parametric amplification of the emitted light [10]. In this situation, a theoretical description of the system is given by considering that only three modes for exciton-polaritons —namely, signal ($\mathbf{0}$), pump (\mathbf{k}_p), and idler ($2\mathbf{k}_p$) —are coherently and macroscopically populated [11]. If \mathbf{k}_p is the wave vector of pumping, the scattering of two \mathbf{k}_p exciton-polaritons results in two other exciton-polaritons with wave vectors $\mathbf{0}$ and $2\mathbf{k}_p$. Considering this dynamics, we can approximate Hamiltonian Eq. (2) by a three-mode Hamiltonian as Eq. (1) with $p_{\mathbf{0}} \equiv a_0$, $p_{\mathbf{k}_p} \equiv a_1$, and $p_{2\mathbf{k}_p} \equiv a_2$. In this way, the coefficients G_{ijkl} are functions of the $V_{\mathbf{k},\mathbf{k}',\mathbf{q}}^{PP}$ and the condition $i + j = k + l$ in Eq. (1) is assured by the conservation of momentum in the second term of Eq. (2).

B. An effective Hamiltonian

The three-mode Hamiltonian Eq. (1) conserves the total number of bosons represented by the observable $\hat{N} \equiv a_0^\dagger a_0 + a_1^\dagger a_1 + a_2^\dagger a_2$. Besides that, the difference between the population of bosons in modes 0 and 2, i.e., the imbalance represented by $\hat{D} \equiv a_0^\dagger a_0 - a_2^\dagger a_2$, is also conserved. These are two constants of motion under the evolution given by Eq. (1). In terms of \hat{N} and \hat{D} operators, we can rewrite Hamiltonian Eq. (1) as

$$H = H_{ND}(\hat{N}, \hat{D}) + H_{eff}(\hat{n}_0, a_0 a_2 a_1^{\dagger 2}), \quad (5)$$

where $\hat{n}_0 \equiv a_0^\dagger a_0$. For convenience and symmetry, we will consider N even and $D = 0$. We can observe that H_{ND} is constant, giving rise only to a global phase in the state of the

system as a function of time. The time evolution depends only on the second part of Eq. (5), an effective Hamiltonian given by

$$H_{\text{eff}} = \hbar\delta\hat{n}_0 + \hbar g(\hat{n}_0)^2 + \hbar[Ga_0^\dagger a_2^\dagger a_1^2 + G^* a_0 a_2 (a_1^\dagger)^2], \quad (6)$$

where $\hbar\delta = E_0 + E_2 - 2E_1 - \hbar G_{0000} - \hbar G_{2222} + 2\hbar G_{1111} + 4\hbar N[G_{1212} + G_{0101} - G_{1111}]$, $g = -8G_{1212} + G_{0000} + 4G_{0202} - 8G_{0101} + 4G_{1111} + G_{2222}$, and $G = 2G_{1102}$. In the next section we study the properties of the spectrum of the above Hamiltonian for different values of parameters G/δ and g/δ .

III. QUANTUM SPECTRUM

In Fig. 1 we observe the eigenvalues E_i ($i = 1, 2, \dots, N/2 + 1$) for the rescaled Hamiltonian $E = H_{\text{eff}}/\hbar\delta$ as a function of the eigenstate index i for different values G/δ of the coupling between the three modes. We take $g/\delta = 0$ [Fig. 1(a)], $g/\delta = 0.003$ [Fig. 1 (b)], and $g/\delta = -0.003$ [Fig. 2], and we choose $N = 500$. In both cases of Fig. 1, the spectra show maximal level densities at energies $E = 0$ and $E = N/2 + (g/\delta)(N/2)^2$, which are inflection points. Moreover, we see that for $g/\delta = 0$ the spectra are always symmetric with respect to the central level and both inflection points move accordingly toward the center as a function of G/δ . For values $g/\delta > 0$, the spectra are asymmetric and the inflection points move separately toward the center as G/δ is varied. For $g/\delta < 0$ [Fig. 2], we observe a more complex behavior with a two-fold degeneracy which disappears for $G/\delta > 0.0005$ [Fig. 2 (a)], but in essence it is similar to the case $g/\delta > 0$, with two asymmetrical inflection points moving separately to the centre of the spectrum (Fig. 2 (b)). When we calculate the mean values of population in mode 0, $\langle n_0 \rangle$, and in mode 1, $\langle n_1 \rangle$, for a degenerate spectrum, we find that, at a degeneracy, there is the possibility of population inversion between modes with the same energy value. In other words, two states with the same energy, $E_i = E_{i+1}$, may have $\langle n_0 \rangle > \langle n_1 \rangle$ or $\langle n_0 \rangle < \langle n_1 \rangle$. Therefore, the degeneracy is characterized by the possibility of reversing the population of modes without altering the state's energy.

We can also observe the behavior of the spectrum in Fig. 3, where maximal level densities appear as minimal differences for adjacent energy levels. It has been shown [26, 28] that in these Curie-Weiss models a quantum phase transition is connected with the level approximation, occurring maximally at these inflection points. We will also see that in

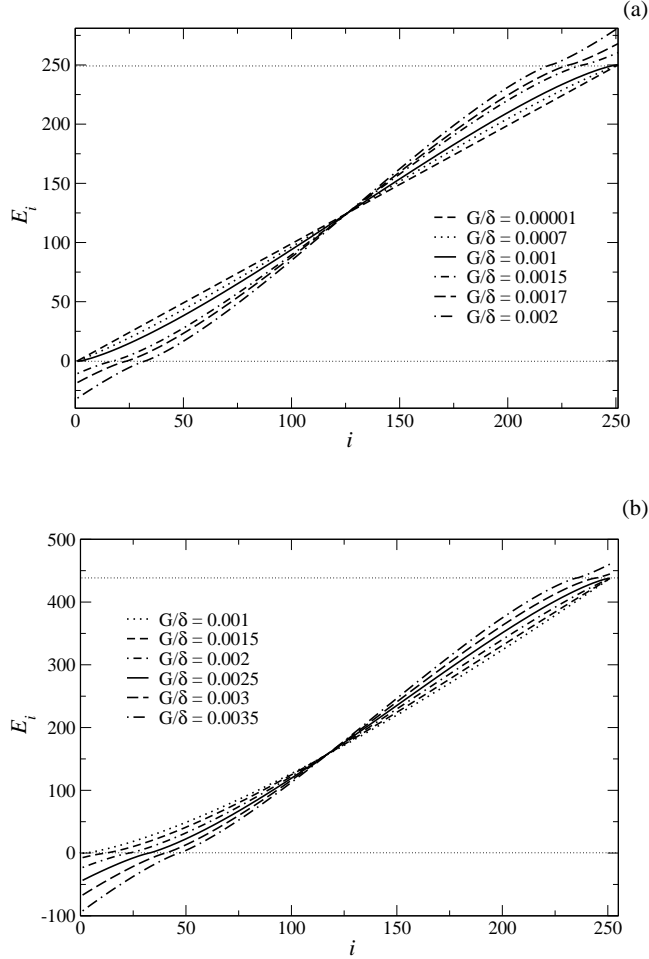


FIG. 1. Energy eigenvalues E_i as a function of the eigenstate index i for $g/\delta = 0$ (a), $g/\delta = 0.003$ (b), $N = 500$, and different values of the three-mode coupling coefficient G/δ . The horizontal dotted lines mark the values $E = 0$ and $E = N/2 + (g/\delta)(N/2)^2$.

the thermodynamic limit the inflection point is associated with a separatrix orbit in the corresponding classical phase space.

IV. CLASSICAL THERMODYNAMIC LIMIT OF THE HAMILTONIAN

The classical analog can be obtained as the thermodynamic limit of Hamiltonian Eq. (6). The first step is the mapping of the operators into a $SU(2)$ algebra by taking

$$J_z \equiv \hat{n}_0 - \frac{\hat{N}}{4}, \text{ and} \quad (7)$$

$$J_+ = J_-^\dagger = \frac{1}{\sqrt{2\hat{n}_0(N - 2\hat{n}_0 + 1)}} a_0^\dagger a_2^\dagger a_1^2. \quad (8)$$

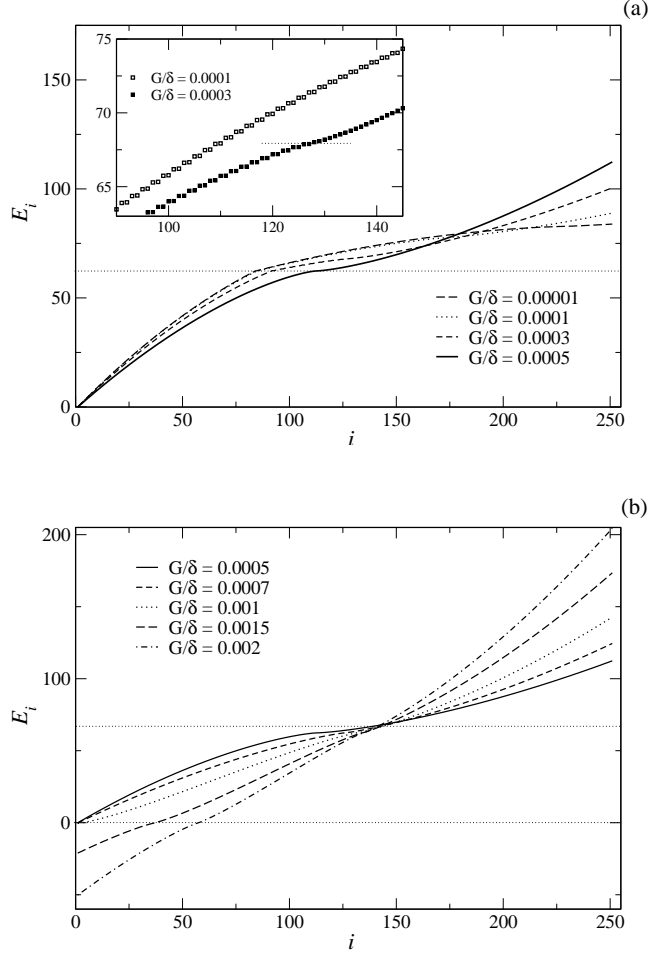


FIG. 2. Energy eigenvalues E_i as a function of the eigenstate index i for $g/\delta = -0.003$, $N = 500$, and different values of the three-mode coupling coefficient G/δ . For $G/\delta < 0.0005$ (a) we observe a two-fold degeneracy which vanishes for $G/\delta > 0.0005$ (b).

With these operators, Hamiltonian Eq. (6) is rewritten as

$$\begin{aligned}
H_{\text{eff}} &= \hbar\delta(J_z + J) + \hbar g(J_z + J)^2 \\
&+ \hbar \left\{ G\sqrt{2(J_z + J)[N - 2(J_z + J) + 1]}J_+ \right. \\
&\left. + G^*J_-\sqrt{2(J_z + J)[N - 2(J_z + J) + 1]} \right\}
\end{aligned} \tag{9}$$

with $J = N/4$.

The following step to the thermodynamic limit is obtained by rescaling the Hamiltonian by the density N/V and taking the limits $N \rightarrow \infty$ and $V \rightarrow \infty$, with the ratio N/V being

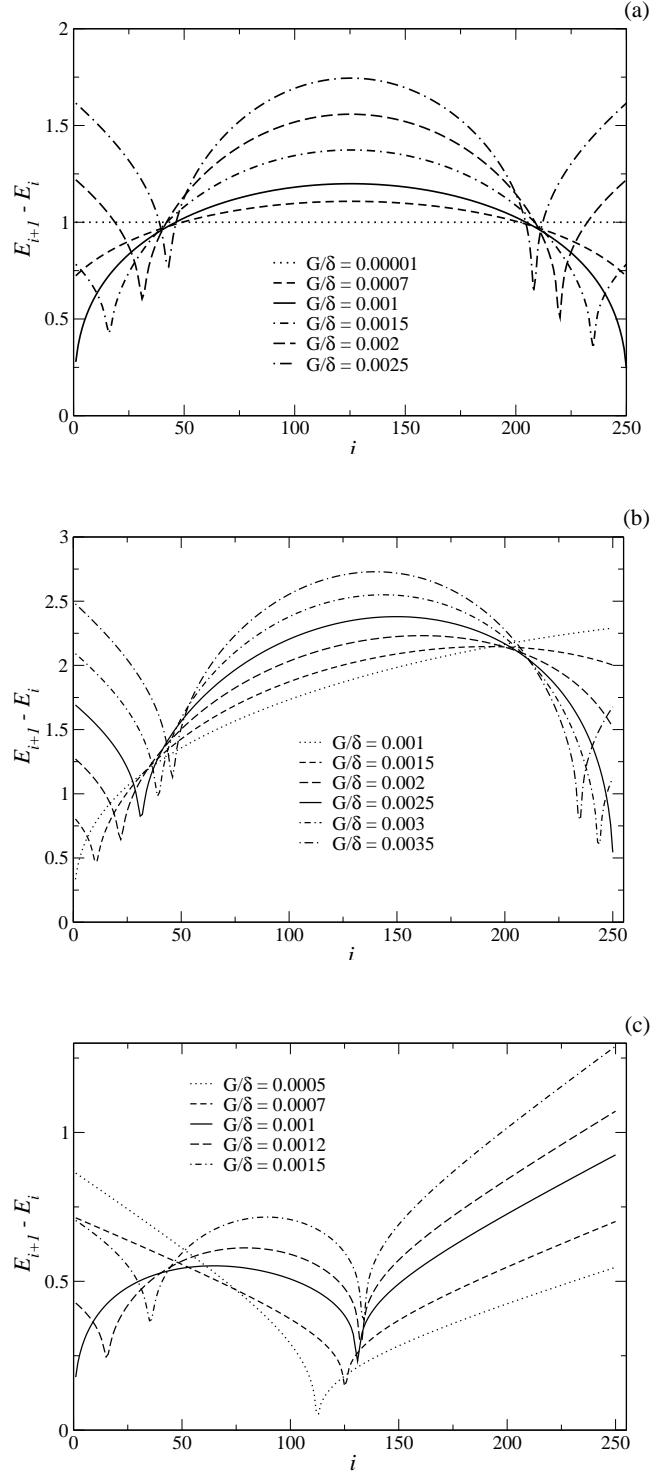


FIG. 3. Difference between adjacent energy eigenvalues $E_{i+1} - E_i$ as a function of the index i for $g/\delta = 0$ (a), $g/\delta = 0.003$ (b), and $g/\delta = -0.003$ (c), $N = 500$, and different values of the three-mode coupling coefficient G/δ .

kept constant. In this limit, the classical variables are provided by the usual definitions [30]

$$j_k = \lim_{J \rightarrow \infty} \frac{J_k}{J}, \quad (k = +, -, z) \quad (10)$$

and

$$j_x = \frac{1}{2}(j_+ + j_-) = \sqrt{1 - j_z^2} \cos \phi, \quad (11)$$

where ϕ and j_z correspond to canonical conjugate variables. The classical Hamiltonian finally obtained is written as

$$h(j_z, \phi) = \delta'(j_z + 1) + g'(j_z + 1)^2 + 4G'(1 - j_z^2) \cos(\phi) \quad (12)$$

with the rescaled parameters $\delta' = \hbar\delta V/4$, $g' = \hbar g NV/16$ and $G' = \hbar G NV/16$.

The classical phase space $\phi \times j_z$ is shown in Figs. 4–7, using, respectively, $g'/\delta' = 0$, $g'/\delta' = 0.375$, and $g'/\delta' = -0.375$ for some given values of the three-mode coupling G'/δ' . As expected, the phase space is periodic in the variable ϕ and j_z is restricted to $-1 \leq j_z \leq 1$. In these figures we can see two different dynamical regimes: closed and open orbits separated by a separatrix corresponding to the classical energies for $j_z = \pm 1$. The closed orbits correspond to classical energies less than $h(j_z = -1)$ or greater than $h(j_z = 1)$. The arising of the separatrix in phase space is associated to the level approximation in the quantum spectrum [26, 28]. This can be seen in the three cases below:

(i) $g'/\delta' = 0$ ($g/\delta = 0$): We observe the appearance of two separatrices for $G'/\delta' > 0.125$ ($G/\delta > 0.001$) next to upper and lower classical energies $h(j_z = 1)$ and $h(j_z = -1)$, while in the quantum spectrum we observe the level approximation in both extreme energies.

(ii) $g'/\delta' = 0.375$ ($g/\delta = 0.003$): We observe the appearance of a separatrix for $G'/\delta' > 0.125$ ($G/\delta > 0.001$) next to the lower classical energy $h(j_z = -1)$ and for $G'/\delta' > 0.3125$ ($G/\delta > 0.0025$) next to the upper classical energy $h(j_z = 1)$, while in the quantum spectrum we observe respective level approximations next to upper and lower energies.

(iii) $g'/\delta' = -0.375$ ($g/\delta = -0.003$): Besides the behavior seen in (ii), we also observe a degeneracy of two classical trajectories with the same energy. This degeneracy disappears for $G'/\delta' > 0.0625$ ($G/\delta > 0.0005$).

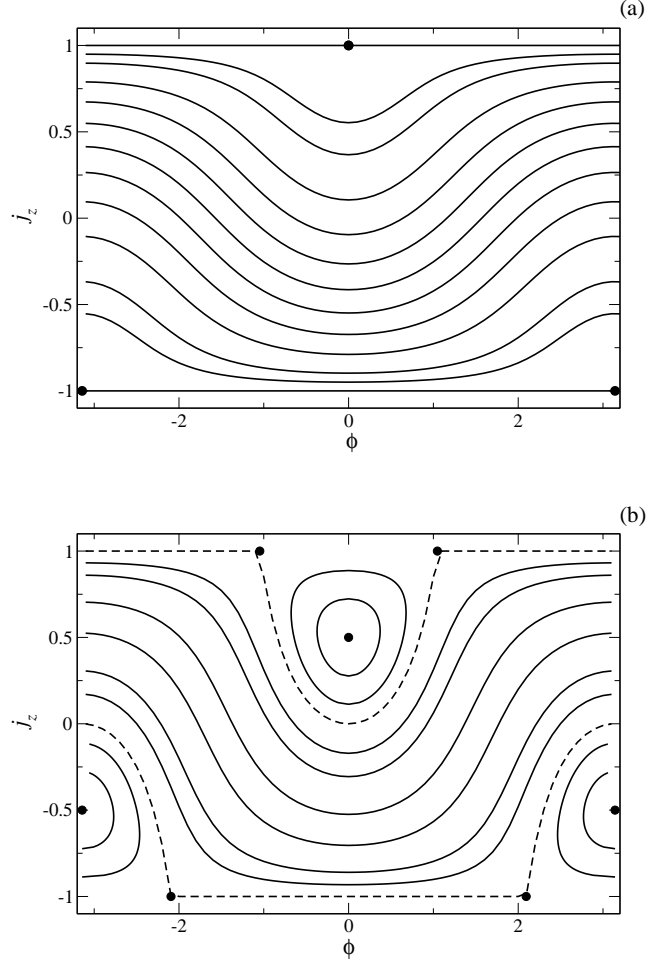


FIG. 4. Phase space $\phi \times j_z$ for $g'/\delta' = 0$, $G'/\delta' = 0.125$ (a), and $G'/\delta' = 0.25$ (b). Rescaled parameters calculated for $N = 500$, $g/\delta = 0$, $G/\delta = 0.001$ (a), and $G/\delta = 0.002$ (b). The critical points of $h(\phi, j_z)$ are signaled by black dots.

The previous aspects can be explained analytically by means of the critical points of the function $h(\phi, j_z)$. These are of two kinds:

—Maxima or minima localized at

$$(\phi, j_z)_{\max, \min} = \left(2n\pi, \frac{\delta' + 2g'}{8G' - 2g'} \right) \quad (13)$$

and

$$(\phi, j_z)_{\max, \min} = \left((2n + 1)\pi, -\frac{\delta' + 2g'}{8G' + 2g'} \right), \quad (14)$$

—Saddle points at

$$(\phi, j_z)_{\text{saddle}} = \left(\arccos \left[\frac{\delta' + 4g'}{8G'} \right], 1 \right) \quad (15)$$

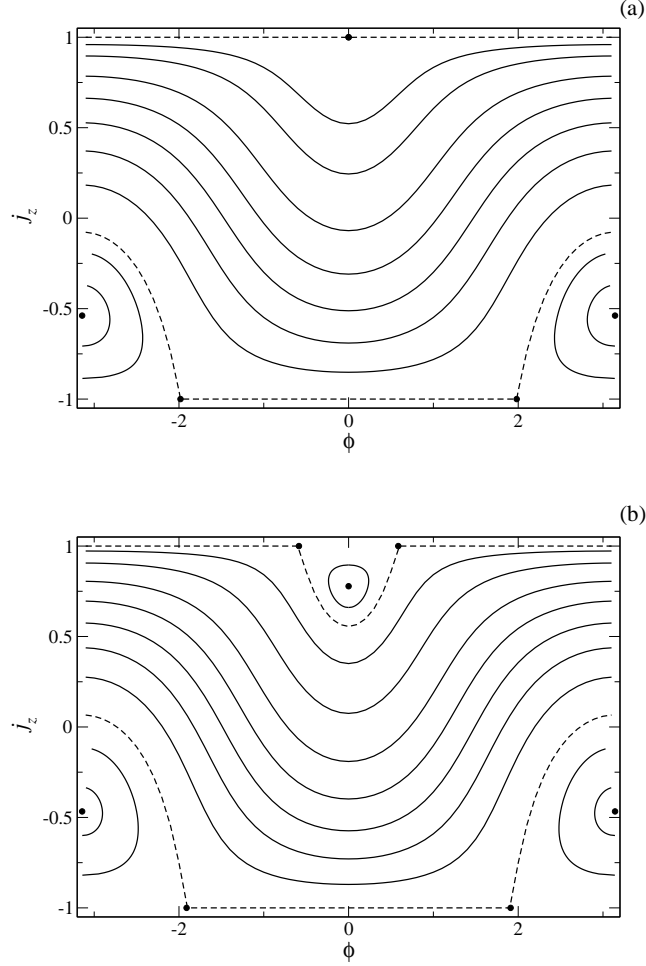


FIG. 5. Phase space $\phi \times j_z$ for $g'/\delta' = 0.375$, $G'/\delta' = 0.3125$ (a), and $G'/\delta' = 0.375$ (b). Rescaled parameters calculated for $N = 500$, $g/\delta = 0.003$, $G/\delta = 0.0025$ (a), and $G/\delta = 0.003$ (b). The critical points of $h(\phi, j_z)$ are signaled by black dots.

and

$$(\phi, j_z)_{\text{saddle}} = \left(\arccos \left[\frac{-\delta'}{8G'} \right], -1 \right). \quad (16)$$

These critical points are shown in Figs. 4–7. The critical points in Eqs. (13) and (14) can be maxima or minima, depending on whether $g'/\delta' \geq 0$ or $g'/\delta' < 0$. The closed orbits are created around the maximum and minimum points. Therefore, the conditions for the existence of these points are the conditions for the arising of the separatrix for upper and lower classical energies. We deduce from the conditions above that we have the arising of the two separatrices starting for the same value of the three-mode coupling $G'/\delta' = 0.125$ when $g'/\delta' = 0$. In the same way, when $g'/\delta' = 0.375$ we have two distinct values of the

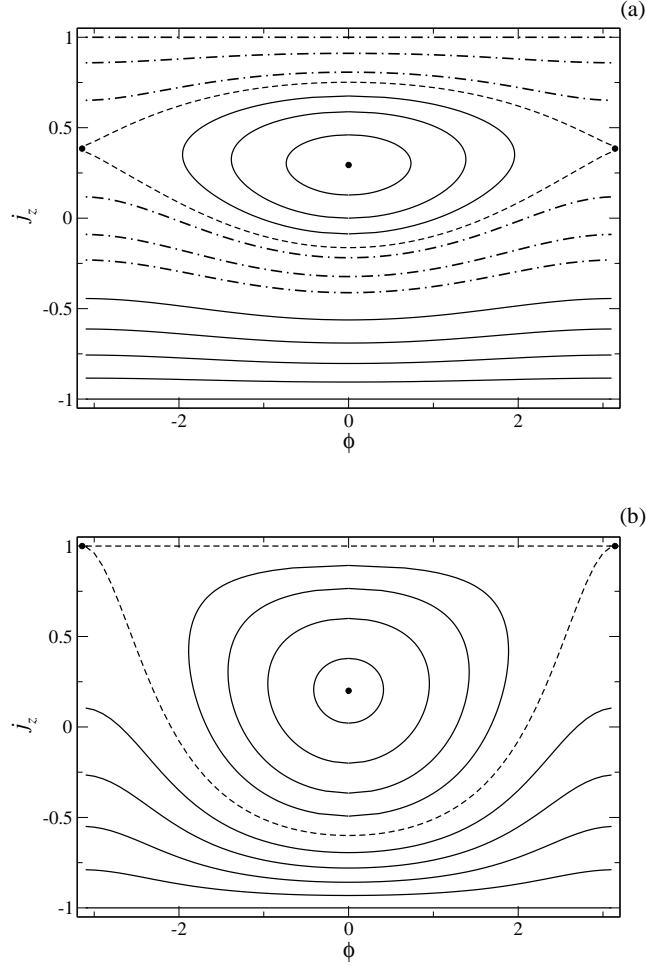


FIG. 6. Phase space $\phi \times j_z$ for $g'/\delta' = -0.375$, $G'/\delta' = 0.0125$ (a), and $G'/\delta' = 0.0625$ (b). Rescaled parameters calculated for $N = 500$, $g/\delta = -0.003$, $G/\delta = 0.0004$ (a), and $G/\delta = 0.0005$ (b). The critical points of $h(\phi, j_z)$ are signaled by black dots and the degenerated open orbits by trace-dotted curves.

three-mode coupling $G'/\delta' = 0.125$ and $G'/\delta' = 0.3125$ for the arising of the separatrix for upper and lower classical energies respectively. We can interpret these values as the critical values of the quantum phase transitions, with the appearance of the closed orbits in phase space signaling the possibility of another physical phase accessible to the system. As it is shown in Figs. 4–7, the arising of this second phase for upper classical energies depends on the value of the parameter g'/δ' . For $g'/\delta' = 0$, the second phase (closed orbits) arises for upper energies when $G'/\delta' \geq 0.125$, while for $g'/\delta' = 0.375$ and -0.375 it occurs for $G'/\delta' \geq 0.3125$ and $G'/\delta' \geq 0$, respectively.

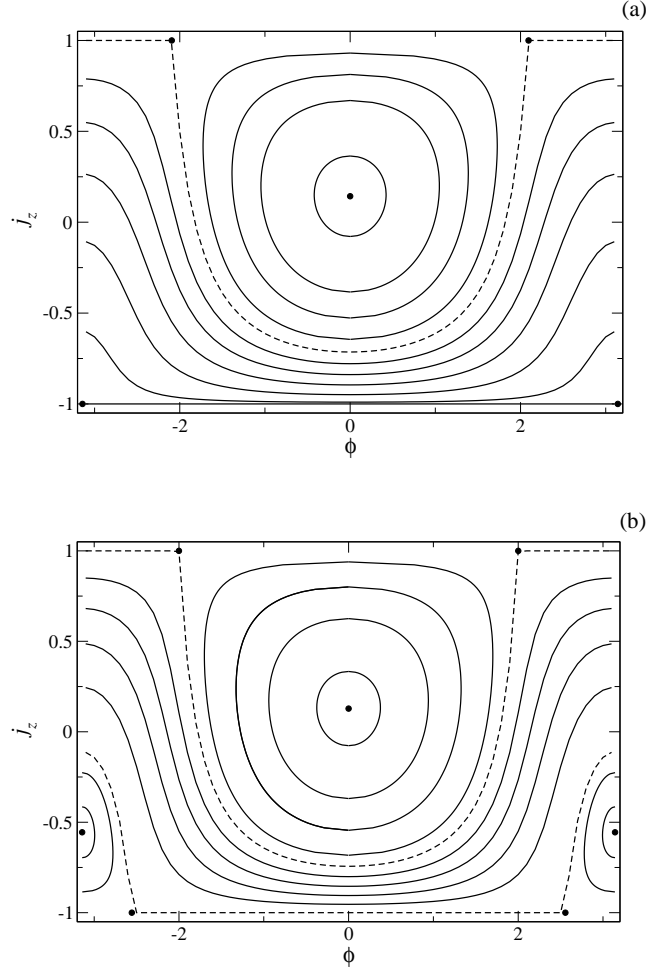


FIG. 7. Phase space $\phi \times j_z$ for $g'/\delta' = -0.375$, $G'/\delta' = 0.125$ (a), and $G'/\delta' = 0.15$ (b). Rescaled parameters calculated for $N = 500$, $g/\delta = -0.003$, $G/\delta = 0.001$ (a), and $G/\delta = 0.002$ (b). The critical points of $h(\phi, j_z)$ are signaled by black dots.

V. QUANTUM PHASE TRANSITION

We can observe characteristics of a quantum phase transition by looking at the properties of the ground state and of the measures of its entanglement [1, 31]. In Fig. 8 we show the average value of the 0-mode population $\langle n_0 \rangle$ and the linear entropy $S = 1 - \text{Tr}[\rho_{n_0}^2]$ for the ground state of the system. Here, ρ_{n_0} stands for the reduced density operator of the 0-mode for the ground state, obtained by tracing out the other modes. We clearly observe two distinct behaviors for these quantities, for $G/\delta < 0.001$ or $G/\delta > 0.001$. This can be associated with the phase transition between the two dynamical regimes of macroscopic self-trapping (MST) and of oscillations (RO). For $G/\delta < 0.001$, the average 0-mode population

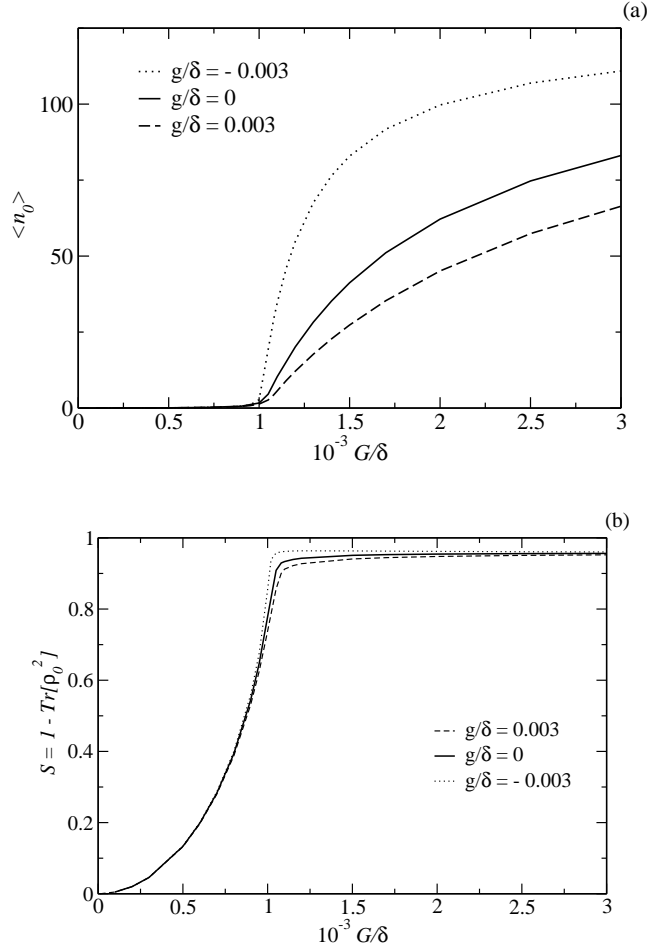


FIG. 8. Average value of population $\langle n_0 \rangle$ (a) and the linear entropy $S = 1 - \text{Tr}[\rho_{n_0}^2]$ of the 0-mode (b) as a function of the three-mode coupling G/δ for the ground-state of the system.

is practically null and we can deduce that the total population of bosons is on average in the 1-mode. This situation characterizes the MST phase in which the bosons remain in a single mode. This more organized phase has a relatively small linear entropy, so a small entanglement. For $G/\delta > 0.001$, the average 0-mode population is non-null and increases with the three-mode coupling. In this situation we can say that the total population of bosons tends on average to be divided among the different modes. This situation characterizes the RO phase in which the bosons do not have a preferred mode and oscillate between them. As the system is in a more disordered situation the linear entropy is larger, and so is the entanglement.

A. Order of the phase transition

We can now discuss the order of the quantum phase transition. Following the usual criterion [1, 31], we can obtain this information by analyzing the behavior of the ground state energy and the entanglement, and their derivatives. Figure 9 shows the behavior of the ground state energy as a function of the three-mode coupling G'/δ' . In the same figure we observe the minimum of the corresponding classical energy $h(j_z, \phi)$, which shows a perfect agreement with the ground state energy rescaled as $E/(N/4)$. Taking the first and second derivatives, we observe that the first derivative is continuous and the second one is discontinuous [Fig. 9 (b)]. In Fig. 10 the first derivative of the linear entropy as a function of the three-mode coupling G'/δ' is shown for different values of the total boson population N . We observe that the curves tend to diverge as $N \rightarrow \infty$ at the critical value $G'/\delta' = 1.25$. Such aspects, i.e., the second derivative of the energy and the first derivative of the entropy, both discontinuous for the ground state, characterize a second order phase transition. We note that a first-order transition would be characterized by a discontinuous first derivative of the ground state energy [1, 31].

B. Phase diagram

We can now construct a phase diagram for the transition. We observe that in the quantum spectrum (Fig. 1) for $G/\delta < 0.001$ the eigenenergies are restricted to values $0 < E < N/2 + (g/\delta)(N/2)^2$, while for $G/\delta > 0.001$ some eigenenergies $E < 0$ and $E > N/2 + (g/\delta)(N/2)^2$ arise. These quantum states correspond precisely to classical closed orbits which arise for $G/\delta > 0.001$. In this way we can associate these quantum states with the second phase of the system and separate the spectrum in different regions for the values $E < 0$ and $E > N/2 + (g/\delta)(N/2)^2$. Varying the three-mode coupling G/δ , we change the number of eigenstates (regions of the spectrum) associated with the second phase. While G/δ increases, the second phase region of the spectrum becomes larger. This phase diagram is shown in Fig. 11, where the vertical axis is a relative index i/i_{\max} of the eigenvalues E_i . The lower curve separates the eigenvalues $E_i < 0$ while the upper curve separates the eigenvalues $E_i > N/2 + (g/\delta)(N/2)^2$. We can observe that for $g/\delta \neq 0$ the arising of the second phase in upper energies is changed. A similar phase diagram had already been done for the Lipkin

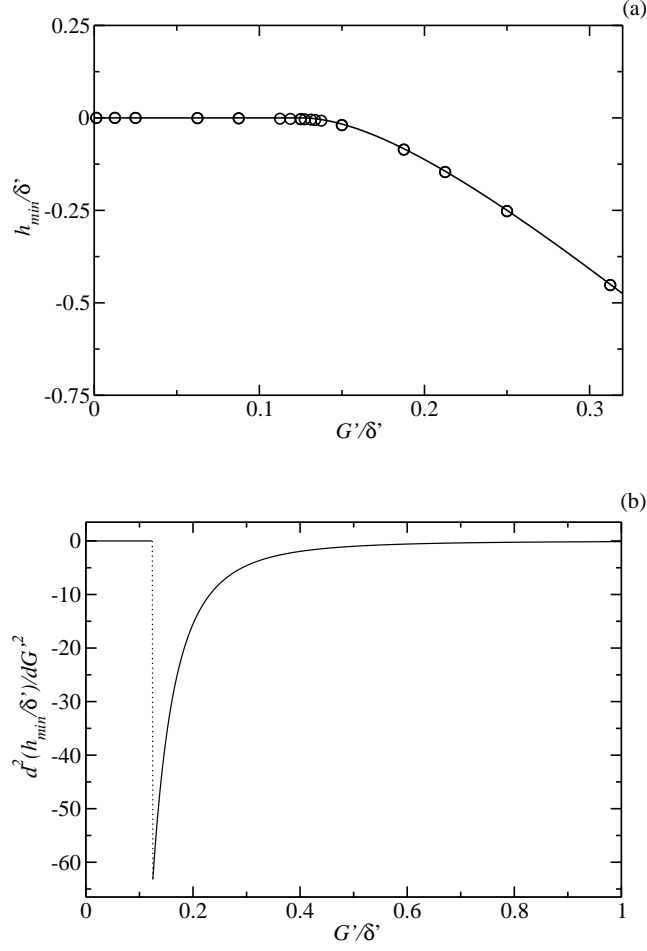


FIG. 9. The ground state energy (a) and its second derivative (b) as a function of the three-mode coupling G'/δ' . In (a) we also observe the ground state energy rescaled as $E/(N/4)$ (circle).

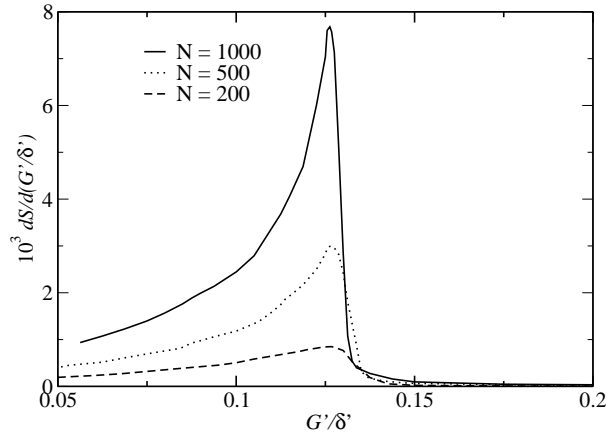


FIG. 10. The first derivative of the linear entropy $S = 1 - Tr[\rho_{n_0}^2]$ as a function of the three-mode coupling G'/δ' for the ground state and different total boson populations $N = 200, 500,$ and 1000 .

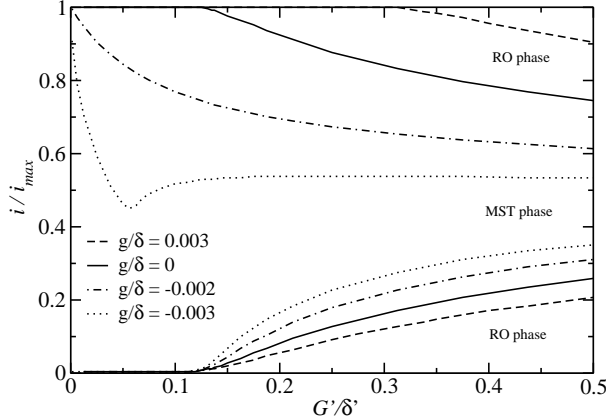


FIG. 11. Phase diagram for $g/\delta = 0.003, 0, -0.002,$ and -0.003 . For each value of g/δ we have two lines: in the middle of the lines the eigenstates are in a phase of macroscopically self-trapping (MST), above and below these lines the eigenstates are in a phase of the regime of oscillations (RO).

model in Ref. [25]. The difference between our three-mode model and the Lipkin model is just the asymmetry due to coefficient g/δ , since the Lipkin model has a symmetric phase diagram. This feature gives rise to a situation in this three-mode model which does not occur in the Lipkin model: the manifestation of the second phase in the upper energies is changed for $g/\delta \neq 0$.

VI. APPLICATION

In the previous sections we have analyzed the behavior of the three-mode Hamiltonian and of its corresponding classical hamiltonian function for different values of the parameters G/δ and g/δ . But until now we have not discussed how we can vary physically these parameters. We will examine below an example for exciton-polaritons in a semiconductor microcavity.

We can use experimental values of an exciton-polariton system at the magic angle configuration to test the results obtained in the previous sections. The values of the parameters G/δ and g/δ in the effective Hamiltonian Eq. (6) can be determined from the parameters $\hbar\Omega_k$ and $V_{\mathbf{k},\mathbf{k}',\mathbf{q}}^{PP}$ in the exciton-polariton Hamiltonian Eq. (2). In Fig. 12 we observe a curve of G/δ as a function of the detuning Δ_0 numerically calculated from experimental values [32]. In this figure we note that the increase in the three-mode coupling due to detuning variation results in phase transition from MST to RO.

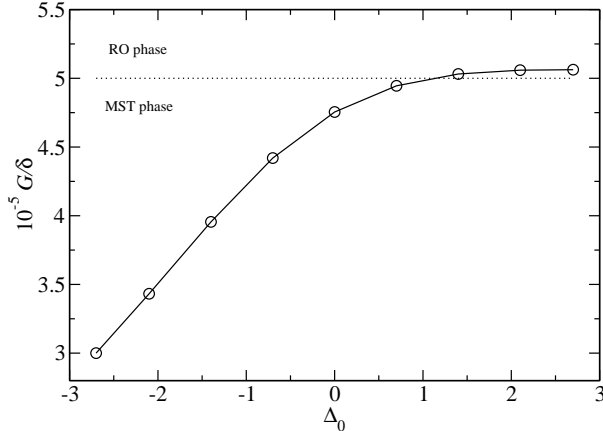


FIG. 12. Numerical value for G/δ as a function of the detuning Δ_0 , calculated from experimental parameters of a semiconductor microcavity [32]. The horizontal dotted line marks the critical value $G/\delta = 0.00005$ for $N = 10^4$.

We emphasize that an exciton-polariton system is a very complex system with numerous features which were not considered in our simple analysis. For example, the coexistence of other system components such as photons, excitons, or bi-excitons, and the consequent conversion between them. Also, there is the non-conservation of total number of particles due to pumping and dissipation in the system. In this way, our work constitutes a first and simple approach to a complex system and is based on features of the macroscopic population of the three exciton-polariton modes at the magic angle configuration. In other words, we have an effective but physically meaningful model.

VII. CONCLUSIONS

The three-mode Hamiltonian studied in this work can be classified in a class of schematic models named Curie-Weiss models. There are many examples of this class as the Lipkin model and the pairing model (both in nuclear physics), the Dicke model for the superradiance, and others. Models in this class share the characteristic of a Hamiltonian which allows an expansion in powers of $1/N$, which in a thermodynamic limit leads to a classical Hamiltonian analysis. In these models a quantum phase transition is signaled by a level approximation near an inflection point of the spectrum. This feature in the classical analysis is signaled by the appearance of a separatrix in the phase space. In the Curie-Weiss class,

the Lipkin model has the particularity of a symmetric level approximation in both upper and lower inflection points of the spectrum. The three-mode Hamiltonian studied here also has this particularity and allows moreover for a situation ($g/\delta \neq 0$) of an asymmetric level approximation in the upper and lower parts of the spectrum. In other words, we can have an asymmetric phase diagram.

The effective Hamiltonian obtained in this work can describe exciton-polaritons in a semiconductor microcavity at the magic angle. In terms of the exciton-polariton system, our results constitute an effective but physically meaningful model. It is a simple approach to this intricate system, based on the macroscopic features of the exciton-polariton population of only three modes.

ACKNOWLEDGMENTS

We would like to thank CNPq (Grant No. 312207/2015-8) and CAPES for financial support. H.M.F., J.G.P.F. and G.Q.P. would like to dedicate this work to the memory of Maria Carolina Nemes.

-
- [1] S. Sachdev, *Quantum Phase Transitions* (Cambridge University Press, Cambridge, 1999).
 - [2] W. H. Zurek, U. Dorner, and P. Zoller, Phys. Rev. Lett. **95**, 105701 (2005); S. Gammelmark and K. Mølmer, New J. Phys. **13**, 053035 (2011); L. Tian, Phys. Rev. A **93**, 043850 (2016).
 - [3] A. Halu, S. Garnerone, A. Vezzani, and G. Bianconi, Phys. Rev. E **87**, 022104 (2013).
 - [4] F. Lingua, G. Mazzarella, and V. Penna, J. Phys. B **49**, 205005 (2016).
 - [5] A. V. Kavokin, J. J. Baumberg, G. Malpuech, and F. P. Laussy, *Microcavities* (Oxford University Press, Oxford, 2007).
 - [6] A. V. Kavokin and G. Malpuech, *Thin Films and Nanostructures: Cavity Polaritons* (Elsevier, Amsterdam, 2003), Vol. 32.
 - [7] J. Keeling and N. G. Berloff, Nature **457**, 273 (2009).
 - [8] J. Kasprzak, M. Richard, S. Kundermann, A. Baas, P. Jeambrun, J. M. J. Keeling, F. M. Marchetti, M. H. Szymańska, R. André, J. L. Staehli, V. Savona, P. B. Littlewood, B. Deveaud, and Le Si Dang, Nature **443**, 409 (2006).

- [9] J. D. Plumhof, T. Stöferle, L. Mai, U. Scherf, and R. F. Mahrt, *Nature Materials* **13**, 247 (2014).
- [10] P. G. Savvidis, J. J. Baumberg, R. M. Stevenson, M. S. Skolnick, D. M. Whittaker, and J. S. Roberts, *Phys. Rev. Lett.* **84**, 1547 (2000).
- [11] C. Ciuti, P. Schwendimann, B. Deveaud, and A. Quattropani, *Phys. Rev. B* **62**, R4825 (2000).
- [12] D. M. Stamper-Kurn, M. R. Andrews, A. P. Chikkatur, S. Inouye, H.-J. Miesner, J. Stenger, and W. Ketterle, *Phys. Rev. Lett.* **80**, 2027 (1998); C. E. Wieman, D. E. Pritchard, and D. J. Wineland, *Rev. Mod. Phys.* **71**, S253 (1999).
- [13] M. H. Anderson, J. R. Ensher, M. R. Matthews, C. E. Wieman, and E. A. Cornell, *Science* **269**, 198 (1995); K. B. Davis, M.-O. Mewes, M. R. Andrews, N. J. van Druten, D. S. Durfee, D. M. Kurn, and W. Ketterle, *Phys. Rev. Lett.* **75**, 3969 (1995).
- [14] J. Denschlag, J. E. Simsarian, D. L. Feder, C. W. Clark, L. A. Collins, J. Cubizolles, L. Deng, E. W. Hagley, K. Helmerson, W. P. Reinhardt, *et al.*, *Science* **287**, 97 (2000); B. P. Anderson, P. C. Haljan, C. A. Regal, D. L. Feder, L. A. Collins, C. W. Clark, and E. A. Cornell, *Phys. Rev. Lett.* **86**, 2926 (2001); G. Lamporesi, S. Donadello, S. Serafini, F. Dalfovo, and G. Ferrari, *Nature Physics* **9**, 656 (2013).
- [15] F. Cataliotti, S. Burger, C. Fort, P. Maddaloni, F. Minardi, A. Trombettoni, A. Smerzi, and M. Inguscio, *Science* **293**, 843 (2001); A. Smerzi, S. Fantoni, S. Giovanazzi, and S. R. Shenoy, *Phys. Rev. Lett.* **79**, 4950 (1997); S. Levy, E. Lahoud, I. Shomroni, and J. Steinhauer, *Nature* **449**, 579 (2007).
- [16] H. Ott, E. de Mirandes, F. Ferlaino, G. Roati, G. Modugno and M. Inguscio, *Phys. Rev. Lett.* **92**, 160601 (2004).
- [17] G.J. Milburn, J. Corney, E. M. Wright, and D. F. Walls, *Phys. Rev. A* **55**, 4318 (1997); M. Albiez, R. Gati, J. Fölling, S. Hunsmann, M. Cristiani, and M. K. Oberthaler, *Phys. Rev. Lett.* **95**, 010402 (2005).
- [18] B. Liu, L.-B. Fu, S.-P. Yang, and J. Liu, *Phys. Rev. A* **75**, 033601 (2007).
- [19] V. F. Viscondi, K. Furuya, and M. C. de Oliveira, *Europhys. Lett.* **90**, 10014 (2010).
- [20] A. Leggett, *Rev. Mod. Phys.* **73**, 307 (2001).
- [21] D. Jaksch, C. Bruder, J. I. Cirac, C. W. Gardiner, and P. Zoller, *Phys. Rev. Lett.* **81**, 3108 (1998).
- [22] R. Paredes, *Phys. Rev. A* **73**, 033616 (2006).

- [23] P. Ziń, B. Oleś, M. Trippenbach, and K. Sacha, Phys. Rev. A **78**, 023620 (2008); P. Buonsante, V. Penna, and A. Vezzani, Phys. Rev. A **82**, 043615 (2010); **84**, 061601(R) (2011); P. Jason, M. Johansson, and K. Kirr, Phys. Rev. E **86**, 016214 (2012).
- [24] G. Vidal, J. I. Latorre, E. Rico, and A. Kitaev, Phys. Rev. Lett. **90**, 227902 (2003).
- [25] W. D. Heiss, F. G. Scholtz, and H. B. Geyer, J. Phys. A: Math. Gen. **38**, 1843 (2005).
- [26] M. Reis, M. O. Terra Cunha, A. C. Oliveira, and M. C. Nemes, Phys. Lett. A **344**, 164 (2005).
- [27] S. Schneider and G. J. Milburn, Phys. Rev. A **65**, 042107 (2002); C. Emary and T. Brandes, Phys. Rev. E **67**, 066203 (2003); M. C. Nemes, K. Furuya, G. Q. Pellegrino, A. C. Oliveira, M. Reis, and L. Sanz, Phys. Lett. A **354**, 60 (2006).
- [28] T. Moreira, G. Q. Pellegrino, J. G. Peixoto de Faria, M. C. Nemes, F. Camargo, and A. F. R. de Toledo Piza, Phys. Rev. E **77**, 051102 (2008); M. C. Figueiredo, T. M. Cotta, G. Q. Pellegrino, Phys. Rev. E **81**, 012104 (2010).
- [29] A. P. Hines, C. M. Dawson, R. H. McKenzie, and G. J. Milburn, Phys. Rev. A **70**, 022303 (2004); G. Engelhardt, V. M. Bastidas, W. Kopylov, and T. Brandes, Phys. Rev. A **91**, 013631 (2015).
- [30] E. H. Lieb, Commun. Math. Phys. **31**, 327 (1973).
- [31] L. A. Wu, M. S. Sarandy, and D. A. Lidar, Phys. Rev. Lett. **93**, 250404 (2004).
- [32] E. A. Cotta and F. M. Matinaga, Phys. Rev. B **76**, 073308 (2007); E. A. Cotta, Ph.D. thesis, Universidade Federal de Minas Gerais, 2008.